

Multiphoton resonances in nitrogen-vacancy defects in diamond

Sergei Masis, Nir Alfasi, Roei Levi, Oleg Shtempluck, and Eyal Buks

Andrew and Erna Viterbi Department of Electrical Engineering, Technion - Haifa 32000, Israel

(Dated: April 10, 2019)

Dense ensembles of nitrogen vacancy (NV) centers in diamond are of interest for various applications including magnetometry, masers, hyperpolarization and quantum memory. All of the applications above may benefit from a non-linear response of the ensemble, and hence multiphoton processes are of importance. We study an enhancement of the NV ensemble multiphoton response due to coupling to a superconducting cavity or to an ensemble of Nitrogen 14 substitutional defects (P1). In the latter case, the increased NV sensitivity allowed us to probe the P1 hyperfine splitting. As an example of an application, an increased responsivity to magnetic field is demonstrated.

PACS numbers: 76.30.Mi, 81.05.ug, 42.50.Pq

I. INTRODUCTION

A two level system (TLS) is perhaps the most extreme manifestation of nonlinear response. Systems composed of TLSs and other elements exhibit a variety of nonlinear dynamical effects including multi-photon resonances (MPR) [1–4], frequency mixing [5–7], fluorescence [8, 9], dynamical instabilities [10, 11], suppression of tunneling [12, 13] and breakdown of the rotating wave approximation [14].

Here we study nonlinear response of an ensemble of nitrogen-vacancy (NV) defects in diamond [15]. Two mechanisms that allow the enhancement of MPR are explored. The first one is based on an electromagnetic cavity mode that is coupled to the spin ensemble [16–23]. The second one is attributed to hyperfine splitting [24] of P1 defects [25–27] and their dipolar coupling to the negatively charged NV defects (NV⁻).

The NV⁻ defect has a spin triplet ground state [28] having relatively long coherence time [29]. The NV⁻ spin state can be initiated via the process of optically-induced spin polarization (OISP) [30, 31] and can be measured using the technique of optical detection of magnetic resonance (ODMR) [32–34]. These properties facilitate a variety of applications including magnetometry [26, 35–41], sensing [29, 36, 42, 43] and quantum information processing [44, 45].

Dipolar coupling between NV⁻ and other spin species in diamond gives rise to intriguing effects including hyperpolarization [46–49] and cross-relaxation [27, 50, 51], and can be exploited for optical detection of spin defects in diamond other than NV⁻ [25, 52–57].

The process of cross-polarization between NV⁻ and P1 defects plays an important role in the MPR mechanism. In general, the efficiency of cross polarization depends on the rate of a competing effect of thermal polarization, which is characterized by the longitudinal spin relaxation rate. At cryogenic temperatures the thermal polarization rate can be significantly reduced, and consequently the efficiency of cross-polarization is enhanced.

II. LOW MAGNETIC FIELD ODMR

A spiral resonator [58] made of 500 nm/10 nm thick Niobium/Aluminum with the inner radius of 0.7 mm and line width and spacing of 20 μ m is fabricated on a Sapphire substrate. Type Ib [110] diamond is irradiated with 2.8 MeV electrons at a dose of 8×10^{18} e/cm², annealed for 2 hours at 900 C° and acid cleaned. The samples assembly (see Fig. 1) is placed at a cryostat with base temperature of 3.6 K and mechanically aligned along the magnetic field of an external superconducting solenoid. The photoluminescence light passes through an array of filters and is collected by a photodiode. A microwave synthesizer is connected directly to a loop antenna (shortened end of a coaxial cable) mounted below the sapphire substrate, and the signal amplitude is 100% modulated with a low frequency sine wave. The same wave is used for the photodiode signal demodulation by a lock-in amplifier. Microwave reflection measurements of the resonator yield resonance frequency $\omega_c = 2\pi \times 276$ MHz, unloaded quality factor $Q = 96$ and critical temperature $T_c = 7$ K. The rather low Q might be explained by the proximity to irradiated diamond. The coupling coefficient g between the resonator and the NV⁻ ensemble is given by [23]

$$g^2 = \frac{\gamma_e^2 \mu_0 \hbar \omega_c \int dr n_S P_z |\mathbf{B}_c|^2 \sin^2 \varphi}{\int dr |\mathbf{B}_c|^2}, \quad (1)$$

where $P_z \approx 0.15$ [57] is the spin polarization, n_S is the NV⁻ ensemble number density, φ is the angle between the NV⁻ axis and the cavity magnetic field \mathbf{B}_c , μ_0 is the free space permeability and $\gamma_e = 2\pi \times 28.03$ GHz T⁻¹ is the electron spin gyromagnetic ratio. Assuming constant P_z throughout the diamond, g is readily calculated by means of numerical simulation [see Fig.1(b)] to be $g = 8$ MHz.

ODMR as a function of magnetic field and frequency is shown in Fig. 2. The dotted lines in Fig. 2 are calculated by numerically diagonalizing the NV⁻ ground state spin triplet Hamiltonian, which is given by [60, 61]

$$\frac{\mathcal{H}_{NV}}{\hbar} = \frac{DS_z^2}{\hbar^2} + \frac{E(S_+^2 + S_-^2)}{2\hbar^2} - \frac{\gamma_e \mathbf{B} \cdot \mathbf{S}}{\hbar}, \quad (2)$$

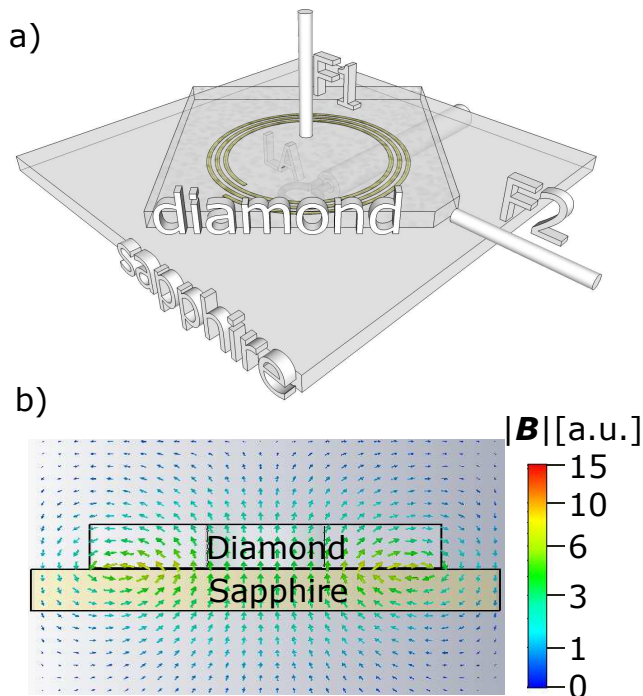


FIG. 1: (a) Experimental setup. The diamond is glued on the top of the spiral resonator, and two multimode optical fibers F1 and F2 are attached to the diamond top and side faces correspondingly. A 532 nm wavelength laser is introduced from one of the fibers, and the photoluminescence is collected from the other, providing a geometrical filtering of the laser light. A microwave loop antenna is placed below the Sapphire at a location optimizing the resonator coupling. (b) Numerical simulation [59] of the spiral fundamental mode magnetic field distribution.

where $\mathbf{S} = (S_x, S_y, S_z)$ is a vector spin $S = 1$ operator, the raising S_+ and lowering S_- operators are defined by $S_{\pm} = S_x \pm iS_y$, the zero field splitting induced by spin-spin interaction D is given by $D = 2\pi \times 2.87$ GHz, the strain-induced splitting E is about $2\pi \times 10$ MHz for our sample and \mathbf{B} is the externally applied magnetic field. The field \mathbf{B} has two contributions $\mathbf{B} = \mathbf{B}_S + \mathbf{B}_L$, where \mathbf{B}_S (\mathbf{B}_L) is the stationary (alternating) field generated by the solenoid (the loop antenna) and is nearly parallel to the lattice direction $[111]$ ($[1\bar{1}0]$).

In a single crystal diamond the NV centers have four different possible orientations. When hyperfine interaction is disregarded each orientation gives rise to a pair of angular resonance frequencies ω_{\pm} , corresponding to the transitions between the spin state with magnetic quantum number 0 and the spin state with magnetic quantum number ± 1 . The dotted line in Fig. 2 having the smallest (largest) frequency for any given magnetic field corresponds to the angular frequency ω_- (ω_+) of the NV⁻ defects having axis in the $[111]$ lattice direction. The other two dotted lines represent the resonances due to the unparallel NV⁻ defects having axis in the lattice di-

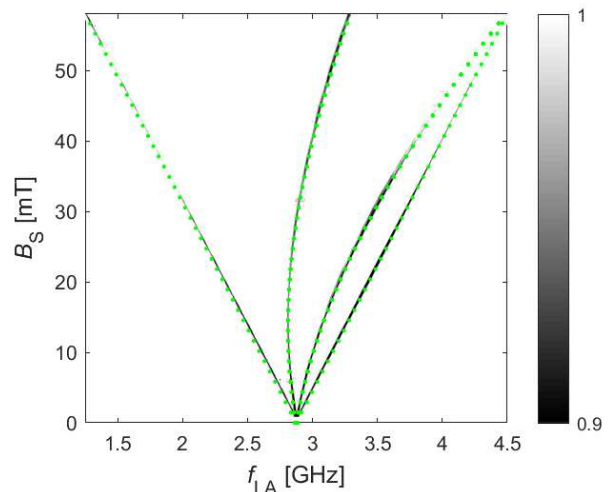


FIG. 2: Low magnetic field ODMR. The overlaid green dotted lines are calculated by diagonalizing the NV⁻ spin Hamiltonian (2). The two nearly straight diagonal curves (leftmost and rightmost) correspond to the NV axis vector nearly parallel to the magnetic field, while the two remaining curves in the middle - to the nearly degenerate three other possible orientations of the NV axis vectors.

rections $[\bar{1}11]$, $[1\bar{1}1]$ or $[11\bar{1}]$.

III. NEAR THE LEVEL ANTI CROSSING

Let ω_a denote the angular frequency ω_- corresponding to the NV⁻ defects having axis in the $[111]$ lattice direction. Consider the case where the magnitude B_S of the solenoid field \mathbf{B}_S is tuned close to the value $D/\gamma_e = 102$ mT. In the vicinity of this level anti-crossing point (LAC) the angular frequency ω_a is approximately given by $\omega_a = \omega_{a0} \sqrt{1 + \eta^2}$, where $\omega_{a0} = \sqrt{2}D\theta_S$ is the lowest value of the angular frequency ω_a , $\theta_S \ll 1$ is the angle between \mathbf{B}_S and the lattice direction $[111]$ ($\theta_S = 1.5^\circ$ and $\omega_{a0}/2\pi = 110$ MHz for the data shown in Figs. 2, 3 and 4), and the dimensionless detuning η is given by $\eta = \gamma_e \delta B_S / \omega_{a0}$, where $\delta B_S = B_S - D/\gamma_e$.

Measured ODMR near the LAC vs. magnetic field B_S and driving frequency $f_{LA} = \omega_{LA}/2\pi$ of the signal injected into the loop antenna is seen in Fig. 3(a). The overlaid white dotted lines are hyperbolas calculated according to $f_{LA} = f_l$, where the frequency of l 'th hyperbola f_l is given by

$$f_l = \omega_a/2\pi l = \omega_{a0} \sqrt{1 + \eta^2} / 2\pi l, \quad (3)$$

where l is an integer from 1 to 10. As can be seen from Fig. 3, along the l 'th hyperbola the largest signal is obtained when the driving frequency is tuned close to $\omega_c/2\pi l$, where $\omega_c/2\pi = 276$ MHz is the cavity resonance frequency. This suggests that the spin MPR are enhanced due to the interaction with the cavity mode.

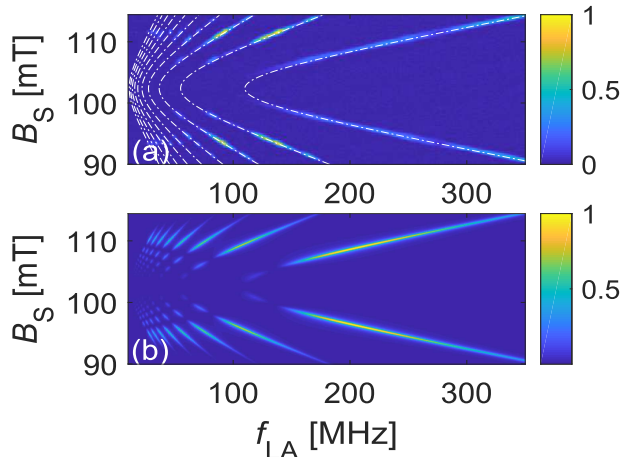


FIG. 3: ODMR with low laser power. (a) The normalized ODMR signal as a function of driving frequency f_{LA} and magnetic field B_S . The overlaid hyperbolas are calculated according to Eq. (3). (b) The normalized steady state polarization $P_z/P_{z,s}$ is calculated according to the Eq. (4) with the following parameters $\omega_c = 2\pi \times 276$ MHz, $\gamma_c = 2.87$ MHz, $\gamma_1 = 20$ Hz and $\gamma_2 = 30$ MHz. In terms of the parameter η the coupling coefficient β_Δ is expressed as $\beta_\Delta = \beta_{\Delta 0}\eta/\sqrt{1+\eta^2}$, where $\beta_{\Delta 0} = 10$.

IV. CAVITY SUPERHARMONIC RESONANCES

The effect of the coupled cavity mode on the spin MPR is discussed in Appendix A. The theoretical model presented in the appendix describes the interplay between two mechanisms. The first one is frequency mixing between transverse and longitudinal spin driving. Near the avoided crossing point the NV^- spin states with magnetic quantum numbers -1 and 0 are mixed, and consequently the amplitudes of transverse and longitudinal driving become strongly dependent on detuning from the avoided crossing point (even when the external driving is kept unchanged). The highly nonlinear nature of the first mechanism results in the generation of harmonics of the externally applied driving frequency. The second mechanism is cavity resonance enhancement, which becomes efficient when one of the generated harmonics coincides with the cavity resonance band. Under appropriate conditions this may give rise to a pronounce cavity-assisted multi-photon resonance.

Consider the case where the frequency of excitation injected into the loop antenna is tuned close to the l 'th superharmonic resonance, i.e. $\omega_a \simeq l\omega_{LA}$, where l is an integer. In that region, the relative change $P_z/P_{z,s}$ in spin polarization in the NV^- triplet ground state is found to be given by [see Eq. (A33) in appendix A]

$$\frac{P_z}{P_{z,s}} = 1 - \frac{\beta_\Delta^2 |\zeta|^2}{1 + \beta_\Delta^2 |\zeta|^2 + \beta_{al}^2}, \quad (4)$$

where [see Eq. (A43)]

$$\zeta = J_l \left(\frac{\omega_b}{\omega_L} \right) \left(1 + \frac{\kappa J_0^2 \left(\frac{\omega_b}{\omega_L} \right) P_{z,s}}{(1 + i\beta_{cl})(1 + i\beta_{al})} \right), \quad (5)$$

ω_b is the amplitude of longitudinal spin driving [see Eq. (A8)], the dimensionless coupling coefficient β_Δ is given by $\beta_\Delta = \omega_\Delta/\sqrt{\gamma_1\gamma_2}$, the dimensionless detuning coefficients β_{cl} and β_{al} are given by $\beta_{cl} = (\omega_c - l\omega_{LA})/\gamma_c$ and $\beta_{al} = (\omega_a - l\omega_{LA})/\gamma_2$, respectively, ω_c is the cavity mode angular frequency, γ_c is the cavity mode damping rate, γ_1 and γ_2 are the longitudinal and transverse spin damping rates, respectively and $\kappa = g^2/\gamma_2\gamma_c$ is the cooperativity parameter. A plot of the normalized steady state polarization $P_z/P_{z,s}$ given by Eq. (4) is shown in Fig. 3(b). The comparison between data and theory yields a qualitative agreement.

V. P1

ODMR data near the LAC with relatively high laser power is shown in Fig. 4. The increase in laser power gives rise to excessive heating, and consequently the superconducting resonator mode becomes undetectable (in a microwave reflectivity measurement) due to a super to normal conduction phase transition of the spiral. The plot contains a variety of peaks all occurring along the above discussed hyperbolas [see Eq. (3)], suggesting that some multiphoton processes continue to exist regardless of the spiral resonator state. Locations of all data peaks are determined by a single frequency denoted by f_m . This can be seen from the cross symbols added to Fig. 4. The frequency $f_{k,l}$ of the k 'th cross symbol overlaid on the l 'th hyperbola in Fig. 4 is given by

$$f_{k,l} = \frac{k}{l} f_m, \quad (6)$$

where the frequency f_m takes the value $f_m = 86$ MHz. This pattern of peaks remains visible with the same value of f_m over a wide range of input microwave power (between 10 and 25 dBm), tenfold laser power attenuation, a few degrees magnetic field misalignments and temperature change. With temperature rising to 30 K, the signal from the higher order hyperbolas disappears, but the f_m beating remains on the main hyperbola. The fact that some of the peaks do not appear at the same frequency for different magnetic fields validates that the pattern is not a measurement artifact of spurious resonances. In addition, the synthesizer signal harmonics were carefully examined with a spectrum analyzer to verify they are all well below the ODMR sensitivity threshold. The measured value of f_m suggests a connection between MPR in the NV^- defects and P1 defect [62–65], as is discussed below.

P1 defect has four locally stable configurations. In each configuration a static Jahn-Teller distortion occurs, and

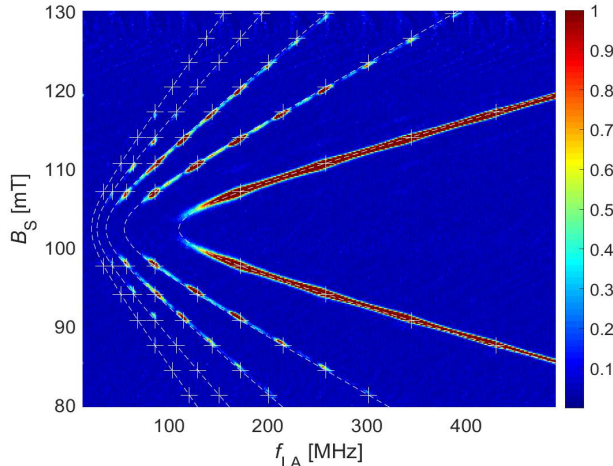


FIG. 4: ODMR with high laser power. The overlaid hyperbolas are calculated according to Eq. (3) and the locations of the cross symbols according to Eq. (6).

an unpaired electron is shared by the nitrogen atom and by one of the four neighboring carbon atoms, which are positioned along one of the lattice directions $[111]$, $[\bar{1}\bar{1}\bar{1}]$, $[\bar{1}\bar{1}1]$ or $[11\bar{1}]$ [20, 46, 53, 54, 66–70].

When both nuclear Zeeman shift and nuclear quadrupole coupling are disregarded, the spin Hamiltonian of a P1 defect is given by [20, 64, 71] $\mathcal{H} = \gamma_e \mathbf{B} \cdot \mathbf{S} + \hbar^{-1} A_{\perp} (S_x I_x + S_y I_y) + \hbar^{-1} A_{\parallel} S_z I_z$, where $\mathbf{S} = (S_x, S_y, S_z)$ is an electronic spin 1/2 vector operator, $\mathbf{I} = (I_x, I_y, I_z)$ is a nuclear spin 1 vector operator, $A_{\parallel} = 2\pi \times 114.03$ MHz and $A_{\perp} = 2\pi \times 81.33$ MHz are respectively the longitudinal and transverse hyperfine parameters, and the z direction corresponds to the diamond $\langle 111 \rangle$ axis. The electron spin resonance at angular frequency $\gamma_e B$ is split due to the interaction with the nuclear spin into three resonances, corresponding to three transitions, in which the nuclear spin magnetic quantum number is conserved [27, 52, 55, 66, 72, 73]. For a magnetic field larger than a few mT the angular resonance frequencies are approximately given by $\gamma_e B$ and $\gamma_e B \pm \omega_{\text{en}}$, where $\omega_{\text{en}}^2 = A_{\parallel}^2 \cos^2 \theta_B + A_{\perp}^2 \sin^2 \theta_B$ and where θ_B is the angle between the magnetic field \mathbf{B} and the P1 axis [62].

Consider the case where \mathbf{B} is in the lattice direction $[111]$. For this case, for 1/4 of the P1 defects $\omega_{\text{en}} = 2\pi \times 114$ MHz, whereas for the other 3/4 of the P1 defects [unparallel to \mathbf{B} having axis in one of the lattice directions $[\bar{1}\bar{1}\bar{1}]$, $[\bar{1}\bar{1}1]$ or $[11\bar{1}]$] $\omega_{\text{en}} = 2\pi \times 85.6$ MHz, close to the observed value of the frequency $f_m = 86$ MHz. The fact that the parallel P1 defects do not have a significant effect on the ODMR data can be attributed to the fact that these defects generate only transverse driving for the NV^- defects having axis parallel to the crystal direction $[111]$, whereas the unparallel P1 defects generate both transverse and longitudinal driving, which in turn allows nonlinear processes of frequency mixing [74].

The effect of dipolar interactions on the measured ODMR signal can be estimated using perturbation theory. To first order the above-discussed hyperfine splitting has no effect. However, as is argued below, a non-vanishing effect is obtained from the second order. Consider a pair of P1 defects with a dipolar coupling to a single NV^- defect [75–81]. Both P1 defects are assumed to be unparallel to \mathbf{B} , i.e. the frequencies of their electronic-like transitions are approximately given by $\gamma_e B/2\pi$ and $\gamma_e B/2\pi \pm 85.6$ MHz. The NV^- defect, on the other hand, is assumed to be nearly parallel to \mathbf{B} , thus having an energy separation of $2\hbar\gamma_e B$ between the spin states with magnetic number ± 1 .

OISP polarizes the NV^- to the $m_s = 0$ state. The required condition for ODMR signal along the l -th hyperbola is achieved by excitation at $\omega_{\text{LA}} = \omega_a/l$, populating the $m_s = -1$ state, which has lower photoluminescence. Let $(m_s^{\text{NV}}, m_s^{\text{P1a}} + m_s^{\text{P1b}}, m_l^{\text{P1a}} + m_l^{\text{P1b}})$ designate a subspace, where m_s^{NV} is the NV^- electronic spin magnetic number, m_s^{P1a} (m_s^{P1b}) is the first (second) P1 electronic spin magnetic number and m_l^{P1a} (m_l^{P1b}) is the first (second) P1 nuclear spin magnetic number. Note that subspaces $(-1, +1, j)$ and $(+1, -1, j)$ for $j \in \{-2, -1, 0, 1, 2\}$, are energetically separated by $\hbar|j|\omega_{\text{en}}$. When $\omega_a = k\omega_{\text{en}}$ for integer k , transitions are stimulated between $(-1, +1, j)$ and $(+1, -1, j)$, further reducing the population of $(0, +1, j)$ and consequently enhancing the ODMR signal.

By employing perturbation theory [82] we find that the effective Rabi rate for these tripolar transitions is roughly given by $\omega_{\text{P1P1NV}} \simeq (n_{\text{S,P1}}/n_{\text{D}})^2 D$, where $n_{\text{S,P1}}$ is the density of P1 defects (which is assumed to be about 100 times larger than the density of NV^- defects, and which can be expressed in terms of the relative concentration of nitrogen atoms p_{N} as $n_{\text{S,P1}} = 1.8 \times 10^{23} \text{ cm}^{-3} p_{\text{N}}$) and where $n_{\text{D}} = 4\pi D/\mu_0\gamma_e^2\hbar = 5.5 \times 10^{22} \text{ cm}^{-3}$. The roughly estimated value of $p_{\text{N}} = 10^{-4}$ yields the rate $\omega_{\text{P1P1NV}}/2\pi \simeq 300$ Hz. In a similar setup [57], at $T = 3.5$ K the maximal OISP rate was found to be $T_{10}^{-1} \approx 200$ Hz and $\gamma_1 \approx 25$ Hz, hence this mechanism is expected to be of significance to a low temperature ODMR measurement.

Note that the transition between $(-1, +1, 0)$ and $(+1, -1, 0)$ does not require additional energy. Stimulated nuclear spin rotation with $\omega_a = k\omega_{\text{en}}/2$ for integer k allows population of $(+1, -1, j_1)$ for $j_1 \in \{-2, -1, 1, 2\}$ via processes of sequential photons absorption. This effect gives rise to the weak peaks on the second ($l = 2$) hyperbola in Fig. 4.

The MPR can be employed for enhancing the responsivity of diamond based magnetometry. Consider a setup with small frequency modulation about a central frequency f_{LA} and photoluminescence signal I demodulation readout. To maximize the responsivity, the bias magnetic field B_{S} and f_{LA} should be set to maximize the derivative $|dI/df_{\text{LA}}|$. As can be seen in Fig. 5, $|dI/df_{\text{LA}}|$ is maximal near the spots associated with P1 hyperfine transitions at the MPR of NV^- . This enhancement is at-

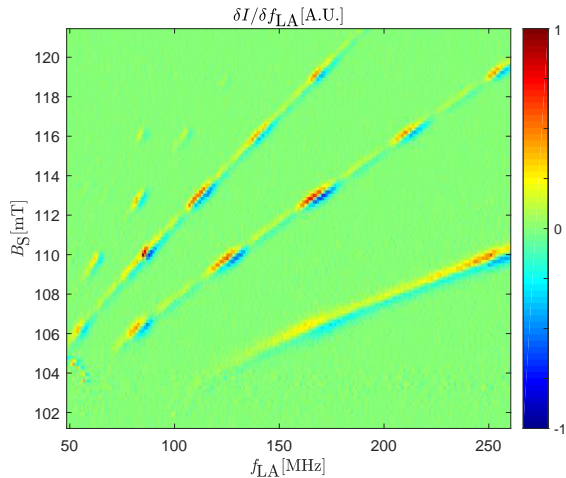


FIG. 5: Derivative of the ODMR photoluminescence signal I with respect to the driving signal frequency f_{LA} at high laser power. The absolute maximal values are achieved not along the single photon curve (bottom right diagonal), but rather at the spots attributed to P1 hyperfine processes on the NV MPR curves (top left diagonals).

tributed to the relatively narrow resonance of the P1 process as compared to the NV MPR.

VI. SUMMARY

Multiphoton processes are surprisingly well measurable in Ib diamonds, making this mode of operation preferable for enhanced sensitivity in multiple applications. Of particular interest is the interaction of the optically measurable and polarizable NV ensemble with the naturally occurring P1 ensemble. The unexpected strength of coupling to the hyperfine transitions of the P1 requires further investigation to determine the nature of the interaction. The NV defects can potentially provide an optical access to a much denser and coherent (nuclear) ensemble of the P1.

VII. ACKNOWLEDGEMENTS

We greatly appreciate fruitful discussions with Paz London, Aharon Blank, Efrat Lifshitz, Vladimir Dyakonov, Sergey Tarasenko, Victor Soltamov, Nadav Katz, Michael Stern and Nir Bar-Gil.

Appendix A: Driven Spins Coupled to a Resonator

Consider a cavity mode coupled to a spin ensemble. The Hamiltonian of the closed system is taken to be given

by

$$\hbar^{-1}\mathcal{H}_0 = \omega_c A^\dagger A + \frac{\mathbf{\Omega} \cdot \mathbf{\Sigma}}{2} + g(A\Sigma_+ + A^\dagger\Sigma_-), \quad (\text{A1})$$

where ω_c is the cavity mode angular frequency, $A^\dagger A$ is a cavity mode number operator, $\mathbf{\Sigma} = (\Sigma_x, \Sigma_y, \Sigma_z)$, the spin operators Σ_z , $\Sigma_+ = (\Sigma_x + i\Sigma_y)/2$ and $\Sigma_- = (\Sigma_x - i\Sigma_y)/2$ are related to the eigenvectors $|\pm\rangle$ of the operator Σ_z by

$$\Sigma_z = |+\rangle\langle+| - |-\rangle\langle-|, \quad (\text{A2})$$

$$\Sigma_+ = |+\rangle\langle-|, \quad (\text{A3})$$

$$\Sigma_- = |-\rangle\langle+|. \quad (\text{A4})$$

The effective magnetic field $\mathbf{\Omega}(t)$ is expressed in terms of the angular frequency ω_T and amplitude ω_1 of transverse driving, the longitudinal magnetic field component $\omega_0(t)$ and transverse one ω_Δ

$$\mathbf{\Omega}(t) = \omega_1 (\cos(\omega_T t) \hat{\mathbf{x}} + \sin(\omega_T t) \hat{\mathbf{y}}) + \omega_0 \hat{\mathbf{z}} + \omega_\Delta \hat{\mathbf{x}}, \quad (\text{A5})$$

or

$$\begin{aligned} \mathbf{\Omega}(t) = \omega_1 (e^{-i\omega_T t} \hat{\mathbf{u}}_+ + e^{i\omega_T t} \hat{\mathbf{u}}_-) + \omega_0(t) \hat{\mathbf{z}} \\ + \omega_\Delta (\hat{\mathbf{u}}_+ + \hat{\mathbf{u}}_-), \end{aligned} \quad (\text{A6})$$

where ω_Δ is a real constant and

$$\hat{\mathbf{u}}_\pm = (1/2) (\hat{\mathbf{x}} \pm i\hat{\mathbf{y}}). \quad (\text{A7})$$

While ω_1 and ω_T are both assumed to be real constants, ω_0 is allowed to vary in time according to

$$\omega_0 = \omega_a - \omega_b \sin(\omega_L t), \quad (\text{A8})$$

where ω_a , ω_b and ω_L are all real constants.

The following Bose

$$[A, A^\dagger] = 1, \quad (\text{A9})$$

and spin

$$[\Sigma_z, \Sigma_+] = 2\Sigma_+, \quad (\text{A10})$$

$$[\Sigma_z, \Sigma_-] = -2\Sigma_-, \quad (\text{A11})$$

$$[\Sigma_+, \Sigma_-] = \Sigma_z, \quad (\text{A12})$$

commutation relations are assumed to hold. The Heisenberg equations of motion are generated according to

$$\frac{dO}{dt} = -i [O, \hbar^{-1}\mathcal{H}_0], \quad (\text{A13})$$

where O is an operator, hence

$$\frac{dA}{dt} = -i\omega_c A - ig\Sigma_-, \quad (\text{A14})$$

$$\frac{d\Sigma_z}{dt} = W_1 \Sigma_+ + W_1^\dagger \Sigma_-, \quad (\text{A15})$$

and

$$\frac{d\Sigma_+}{dt} = i\omega_0\Sigma_+ - \frac{W_1^\dagger}{2}\Sigma_z, \quad (\text{A16})$$

where

$$W_1 = -i(\omega_1 e^{-i\omega_{\text{T}}t} + \omega_\Delta + 2gA). \quad (\text{A17})$$

Averaging

$$\langle A \rangle = \alpha, \quad (\text{A18})$$

$$\langle \Sigma_z \rangle = P_z, \quad (\text{A19})$$

$$\langle \Sigma_\pm \rangle = P_\pm, \quad (\text{A20})$$

and introducing damping leads to

$$\frac{d\alpha}{dt} = -(i\omega_c + \gamma_c)\alpha - igP_-, \quad (\text{A21})$$

$$\frac{dP_z}{dt} = \Omega_1 P_+ + \Omega_1^* P_- - \gamma_1 (P_z - P_{z,s}), \quad (\text{A22})$$

and

$$\frac{dP_+}{dt} = i\omega_0 P_+ - \frac{\Omega_1^*}{2} P_z - \gamma_2 P_+, \quad (\text{A23})$$

where γ_c is the cavity mode damping rate, γ_1 and γ_2 are the longitudinal and transverse spin damping rates, respectively, and where

$$\Omega_1 = -i(\omega_1 e^{-i\omega_{\text{T}}t} + \omega_\Delta + 2g\alpha). \quad (\text{A24})$$

For our experimental conditions the term proportional to ω_1 in Eq. (A24) can be disregarded.

The effect of OISP can be accounted for by adjusting the values of the longitudinal damping rate γ_1 and steady state polarization $P_{z,s}$ and make them both dependent on laser intensity [23, 32]. In this approach γ_1 is given by $\gamma_1 = \gamma_{1\text{T}} + \gamma_{1\text{O}}$, where $\gamma_{1\text{T}}$ is the rate of thermal relaxation and $\gamma_{1\text{O}}$ is the rate of OISP (proportional to laser intensity), and the averaged value of steady state polarization $P_{z,s}$ is given by

$$P_{z,s} = \frac{\gamma_{1\text{T}} P_{z,\text{ST}} + \gamma_{1\text{O}} P_{z,\text{SO}}}{\gamma_1}. \quad (\text{A25})$$

While $P_{z,\text{ST}}$ represents the steady state polarization in the limit $\gamma_{1\text{T}} \gg \gamma_{1\text{O}}$ (i.e. when OISP is negligibly small), the value is $P_{z,\text{SO}}$ for the other extreme case of $\gamma_{1\text{O}} \gg \gamma_{1\text{T}}$ (i.e. when thermal relaxation is negligibly small).

By employing the transformation

$$P_+ = e^{i\theta_d} P_{d+}, \quad (\text{A26})$$

where

$$\theta_d = \int^t dt' [\omega_0(t') + \Delta], \quad (\text{A27})$$

and where Δ is a real constant (to be determined later), Eqs. (A21), (A22) and (A23) become

$$\frac{d\alpha}{dt} = -(i\omega_c + \gamma_c)\alpha - ig \left(\frac{\omega_\Delta \zeta}{\Omega_1} \right)^* P_{d+}^*, \quad (\text{A28})$$

$$\frac{dP_z}{dt} = \omega_\Delta (\zeta P_{d+} + \zeta^* P_{d+}^*) - \gamma_1 (P_z - P_{z,s}), \quad (\text{A29})$$

and

$$\frac{dP_{d+}}{dt} = -i\Delta P_{d+} - \frac{\omega_\Delta \zeta^*}{2} P_z - \gamma_2 P_{d+}, \quad (\text{A30})$$

where

$$\zeta = \frac{\Omega_1}{\omega_\Delta} e^{i\theta_d}. \quad (\text{A31})$$

When ζ is treated as a constant the steady state solution of Eqs. (A29) and (A30) reads

$$P_{d+} = \frac{\omega_\Delta \zeta^* P_z}{2(-i\Delta - \gamma_2)}, \quad (\text{A32})$$

and

$$\frac{P_z}{P_{z,s}} = 1 - \frac{\frac{|\omega_\Delta \zeta|^2}{\gamma_1 \gamma_2}}{1 + \frac{|\omega_\Delta \zeta|^2}{\gamma_1 \gamma_2} + \frac{\Delta^2}{\gamma_2^2}}. \quad (\text{A33})$$

With the help of the Jacobi-Anger expansion, which is given by

$$\exp(iz \cos \theta) = \sum_{n=-\infty}^{\infty} i^n J_n(z) e^{in\theta}, \quad (\text{A34})$$

one obtains [see Eqs. (A8) and (A31)]

$$\zeta = \frac{\Omega_1}{\omega_\Delta} e^{-\frac{i\omega_b}{\omega_L}} \sum_{l'=-\infty}^{\infty} i^{l'} J_{l'} \left(\frac{\omega_b}{\omega_L} \right) e^{i(\omega_a + \Delta + l'\omega_L)t}. \quad (\text{A35})$$

Consider the case where $\omega_a \simeq l\omega_L$, where l is an integer. For this case the detuning Δ is chosen to be given by $\Delta = l\omega_L - \omega_a$, and consequently ζ becomes

$$\zeta = \frac{\Omega_1}{\omega_\Delta} e^{-\frac{i\omega_b}{\omega_L}} \sum_{l'=-\infty}^{\infty} i^{l'} J_{l'} \left(\frac{\omega_b}{\omega_L} \right) e^{i(l+l')\omega_L t}. \quad (\text{A36})$$

The driving term of Eq. (A28) $-ig(\omega_\Delta \zeta / \Omega_1)^* P_{d+}^*$ is approximated by keeping only the term $l' = 0$ in Eq. (A36). When P_{d+}^* is treated as a constant Eq. (A28) yields a steady state solution given by $\alpha = \alpha_0 e^{-il\omega_L t}$, where

$$\alpha_0 = -\frac{ige^{\frac{i\omega_b}{\omega_L}} J_0 \left(\frac{\omega_b}{\omega_L} \right) P_{d+}^*}{\gamma_c (1 + i\beta_{cl})}, \quad (\text{A37})$$

and where

$$\beta_{cl} = \frac{\omega_c - l\omega_L}{\gamma_c}. \quad (\text{A38})$$

To lowest non vanishing order in the coupling g the coefficient P_{d+}^* in Eq. (A37) is evaluated using Eq. (A32) by keeping only the term $l' = -l$ in Eq. (A36) and keeping only the term $-i\omega_\Delta$ in Eq. (A24)

$$P_{d+}^* = \frac{i^{1-l} e^{-\frac{i\omega_b}{\omega_L}} \omega_\Delta J_{-l} \left(\frac{\omega_b}{\omega_L} \right) P_{z,s}}{2\gamma_2 (1 + i\beta_{al})}, \quad (\text{A39})$$

where

$$\beta_{al} = \frac{\omega_a - l\omega_L}{\gamma_2}, \quad (\text{A40})$$

and thus [see Eq. (A37)]

$$\alpha_0 = -\frac{i^{2-l} g \omega_\Delta J_0 \left(\frac{\omega_b}{\omega_L} \right) J_{-l} \left(\frac{\omega_b}{\omega_L} \right) P_{z,s}}{\gamma_c \gamma_2 2(1 + i\beta_{cl})(1 + i\beta_{al})}. \quad (\text{A41})$$

It is assumed that the dominant contribution of ζ to the equation of motion (A29) and (A30) comes from a

term, which is labelled as ζ_a , which is given by [see Eqs. (A24) and (A36)]

$$ie^{\frac{i\omega_b}{\omega_L}} \zeta_a = i^{-l} J_{-l} \left(\frac{\omega_b}{\omega_L} \right) + \frac{2g\alpha_0}{\omega_\Delta} J_0 \left(\frac{\omega_b}{\omega_L} \right). \quad (\text{A42})$$

With the help of Eq. (A41) this becomes

$$i^{1+l} e^{\frac{i\omega_b}{\omega_L}} \zeta_a = J_{-l} \left(\frac{\omega_b}{\omega_L} \right) \left(1 + \frac{\kappa J_0^2 \left(\frac{\omega_b}{\omega_L} \right) P_{z,s}}{(1 + i\beta_{cl})(1 + i\beta_{al})} \right), \quad (\text{A43})$$

where the cooperativity parameter κ is given by

$$\kappa = \frac{g^2}{\gamma_2 \gamma_c}. \quad (\text{A44})$$

The above results (A33) and (A43) lead to Eq. (4) in main text for the steady state polarization.

-
- [1] J. H. Shirley, *Physical Review* **138**, B979 (1965).
[2] D. M. Berns, W. D. Oliver, S. O. Valenzuela, A. V. Shytov, K. K. Berggren, L. S. Levitov, and T. P. Orlando, *Physical Review Letters* **97**, 150502 (pages 4) (2006).
[3] R. Tycko and S. Opella, *The Journal of chemical physics* **86**, 1761 (1987).
[4] F. H. Faisal, *Theory of multiphoton processes* (Springer Science & Business Media, 2013).
[5] L. Childress and J. McIntyre, *Physical Review A* **82**, 033839 (2010).
[6] H. Chen, E. MacQuarrie, and G. Fuchs, *Physical review letters* **120**, 167401 (2018).
[7] H. Mamin, M. Sherwood, M. Kim, C. Rettner, K. Ohno, D. Awschalom, and D. Rugar, *Physical review letters* **113**, 030803 (2014).
[8] B. Mollow, in *Coherence and Quantum Optics* (Springer, 1973), pp. 525–532.
[9] H. Freedhoff and T. Quang, *Physical review letters* **72**, 474 (1994).
[10] J. WEBER, *Rev. Mod. Phys.* **31**, 681 (1959).
[11] M. A. Armen and H. Mabuchi, *Physical Review A* **73**, 063801 (2006).
[12] F. Grossmann, T. Dittrich, P. Jung, and P. Hänggi, *Physical review letters* **67**, 516 (1991).
[13] H. Lignier, C. Sias, D. Ciampini, Y. Singh, A. Zenesini, O. Morsch, and E. Arimondo, *Physical review letters* **99**, 220403 (2007).
[14] G. Fuchs, V. Dobrovitski, D. Toyli, F. Heremans, and D. Awschalom, *Science* p. 1181193 (2009).
[15] M. W. Doherty, N. B. Manson, P. Delaney, F. Jelezko, J. Wrachtrup, and L. C. Hollenberg, *Physics Reports* **528**, 1 (2013).
[16] X. Zhu, S. Saito, A. Kemp, K. Kakuyanagi, S.-i. Karimoto, H. Nakano, W. J. Munro, Y. Tokura, M. S. Everitt, K. Nemoto, et al., *Nature* **478**, 221 (2011).
[17] Y. Kubo, F. Ong, P. Bertet, D. Vion, V. Jacques, D. Zheng, A. Dréau, J.-F. Roch, A. Auffèves, F. Jelezko, et al., *Physical review letters* **105**, 140502 (2010).
[18] Y. Kubo, C. Grezes, A. Dewes, T. Umeda, J. Isoya, H. Sumiya, N. Morishita, H. Abe, S. Onoda, T. Ohshima, et al., *Physical review letters* **107**, 220501 (2011).
[19] R. Amsüss, C. Koller, T. Nöbauer, S. Putz, S. Rotter, K. Sandner, S. Schneider, M. Schramböck, G. Steinhäuser, H. Ritsch, et al., *Phys. Rev. Lett.* **107**, 060502 (2011).
[20] D. Schuster, A. Sears, E. Ginossar, L. DiCarlo, L. Frunzio, J. Morton, H. Wu, G. Briggs, B. Buckley, D. Awschalom, et al., *Physical review letters* **105**, 140501 (2010).
[21] K. Sandner, H. Ritsch, R. Amsüss, C. Koller, T. Nöbauer, S. Putz, J. Schmiedmayer, and J. Majer, *Physical Review A* **85**, 053806 (2012).
[22] C. Grezes, B. Julsgaard, Y. Kubo, M. Stern, T. Umeda, J. Isoya, H. Sumiya, H. Abe, S. Onoda, T. Ohshima, et al., *Physical Review X* **4**, 021049 (2014).
[23] N. Alfasi, S. Masis, R. Winik, D. Farfurnik, O. Shtempler, N. Bar-Gill, and E. Buks, *Physical Review A* **97**, 063808 (2018).
[24] G. A. Álvarez, C. O. Bretschneider, R. Fischer, P. London, H. Kanda, S. Onoda, J. Isoya, D. Gershoni, and L. Frydman, *Nature communications* **6**, 8456 (2015).
[25] E. Kamp, B. Carvajal, and N. Samarth, *Physical Review B* **97**, 045204 (2018).
[26] A. Sushkov, I. Lovchinsky, N. Chisholm, R. L. Walsworth, H. Park, and M. D. Lukin, *Physical review letters* **113**, 197601 (2014).
[27] C. Belthangady, N. Bar-Gill, L. M. Pham, K. Arai, D. Le Sage, P. Cappellaro, and R. L. Walsworth, *Physical review letters* **110**, 157601 (2013).
[28] M. Doherty, F. Dolde, H. Fedder, F. Jelezko, J. Wrachtrup, N. Manson, and L. Hollenberg, *Physical Review B* **85**, 205203 (2012).
[29] G. Balasubramanian, P. Neumann, D. Twitchen, M. Markham, R. Kolesov, N. Mizuochi, J. Isoya,

- J. Achard, J. Beck, J. Tessler, et al., *Nature materials* **8**, 383 (2009).
- [30] L. Robledo, H. Bernien, T. van der Sar, and R. Hanson, *New Journal of Physics* **13**, 025013 (2011).
- [31] D. Redman, S. Brown, R. Sands, and S. Rand, *Physical review letters* **67**, 3420 (1991).
- [32] C. S. Shin, C. E. Avalos, M. C. Butler, D. R. Trease, S. J. Seltzer, J. P. Mustonen, D. J. Kennedy, V. M. Acosta, D. Budker, A. Pines, et al., *Journal of Applied Physics* **112**, 124519 (2012).
- [33] R. Chapman and T. Plakhotnik, *Chemical Physics Letters* **507**, 190 (2011).
- [34] A. Gruber, A. Dräbenstedt, C. Tietz, L. Fleury, J. Wrachtrup, and C. Von Borczyskowski, *Science* **276**, 2012 (1997).
- [35] J. Maze, P. Stanwix, J. Hodges, S. Hong, J. Taylor, P. Cappellaro, L. Jiang, M. G. Dutt, E. Togan, A. Zibrov, et al., *Nature* **455**, 644 (2008).
- [36] V. Acosta, E. Bauch, M. Ledbetter, A. Waxman, L.-S. Bouchard, and D. Budker, *Physical review letters* **104**, 070801 (2010).
- [37] G. Balasubramanian, I. Chan, R. Kolesov, M. Al-Hmoud, J. Tisler, C. Shin, C. Kim, A. Wojcik, P. R. Hemmer, A. Krueger, et al., *Nature* **455**, 648 (2008).
- [38] T. Wolf, P. Neumann, K. Nakamura, H. Sumiya, T. Ohshima, J. Isoya, and J. Wrachtrup, *Physical Review X* **5**, 041001 (2015).
- [39] H. Mamin, M. Kim, M. Sherwood, C. Rettner, K. Ohno, D. Awschalom, and D. Rugar, *Science* **339**, 557 (2013).
- [40] M. Pelliccione, A. Jenkins, P. Ovartchaiyapong, C. Reetz, E. Emmanouilidou, N. Ni, and A. C. B. Jayich, *Nature nanotechnology* **11**, 700 (2016).
- [41] L. Rondin, J.-P. Tetienne, S. Rohart, A. Thiaville, T. Hingant, P. Spinicelli, J.-F. Roch, and V. Jacques, *Nature communications* **4**, 2279 (2013).
- [42] F. Dolde, H. Fedder, M. W. Doherty, T. Nöbauer, F. Rempp, G. Balasubramanian, T. Wolf, F. Reinhard, L. Hollenberg, F. Jelezko, et al., *Nature Physics* **7**, 459 (2011).
- [43] F. Jelezko, T. Gaebel, I. Popa, A. Gruber, and J. Wrachtrup, *Physical review letters* **92**, 076401 (2004).
- [44] P. C. Maurer, G. Kucsko, C. Latta, L. Jiang, N. Y. Yao, S. D. Bennett, F. Pastawski, D. Hunger, N. Chisholm, M. Markham, et al., *Science* **336**, 1283 (2012).
- [45] J. Cai, F. Jelezko, N. Katz, A. Retzker, and M. B. Plenio, *New Journal of Physics* **14**, 093030 (2012).
- [46] S. Takahashi, R. Hanson, J. van Tol, M. S. Sherwin, and D. D. Awschalom, *Physical review letters* **101**, 047601 (2008).
- [47] R. Fischer, C. O. Bretschneider, P. London, D. Budker, D. Gershoni, and L. Frydman, *Physical review letters* **111**, 057601 (2013).
- [48] R. Fischer, A. Jarmola, P. Kehayias, and D. Budker, *Physical Review B* **87**, 125207 (2013).
- [49] H.-J. Wang, C. S. Shin, C. E. Avalos, S. J. Seltzer, D. Budker, A. Pines, and V. S. Bajaj, *Nature communications* **4**, 1940 (2013), article number: 1940.
- [50] I. Solomon, *Physical Review* **99**, 559 (1955).
- [51] M. Loretz, H. Takahashi, T. F. Segawa, J. M. Boss, and C. L. Degen, *Physical Review B* **95**, 064413 (2017).
- [52] M. Simanovskaia, K. Jensen, A. Jarmola, K. Aulenbacher, N. Manson, and D. Budker, *Physical Review B* **87**, 224106 (2013).
- [53] H. Clevenson, E. H. Chen, F. Dolde, C. Teale, D. Englund, and D. Braje, *Phys. Rev. A* **94**, 021401 (2016).
- [54] H.-J. Wang, C. S. Shin, S. J. Seltzer, C. E. Avalos, A. Pines, and V. S. Bajaj, *Nature communications* **5**, 4135 (2014).
- [55] L. Hall, P. Kehayias, D. Simpson, A. Jarmola, A. Stacey, D. Budker, and L. Hollenberg, *Nature communications* **7**, 10211 (2016).
- [56] C. M. Purser, V. P. Bhallamudi, C. S. Wolfe, H. Yusuf, B. A. McCullian, C. Jayaprakash, M. E. Flatté, and P. C. Hammel, arXiv:1802.09635 (2018).
- [57] N. Alfasi, S. Masis, O. Shtempluck, and E. Buks, arXiv:1904.02911 [quant-ph] (2019).
- [58] C. Kurter, A. P. Zhuravel, J. Abrahams, C. L. Bennett, A. V. Ustinov, and S. M. Anlage, *IEEE Transactions on Applied Superconductivity* **21**, 709 (2011).
- [59] CST of America, *Cst studio* (2019).
- [60] P. Ovartchaiyapong, K. W. Lee, B. A. Myers, and A. C. B. Jayich, arXiv:1403.4173 (2014).
- [61] E. MacQuarrie, T. Gosavi, N. Jungwirth, S. Bhave, and G. Fuchs, *Physical review letters* **111**, 227602 (2013).
- [62] W. Smith, P. Sorokin, I. Gelles, and G. Lasher, *Physical Review* **115**, 1546 (1959).
- [63] R. Cook and D. Whiffen, *Proceedings of the Royal Society of London A: Mathematical, Physical and Engineering Sciences* **295**, 99 (1966).
- [64] J. Loubser and J. van Wyk, *Reports on Progress in Physics* **41**, 1201 (1978).
- [65] R. Barklie and J. Guven, *Journal of Physics C: Solid State Physics* **14**, 3621 (1981).
- [66] R. Hanson, V. Dobrovitski, A. Feiguin, O. Gywat, and D. Awschalom, *Science* **320**, 352 (2008).
- [67] D. A. Broadway, J. D. Wood, L. T. Hall, A. Stacey, M. Markham, D. A. Simpson, J.-P. Tetienne, and L. C. Hollenberg, arXiv:1607.04006 (2016).
- [68] J. Shim, B. Nowak, I. Niemeyer, J. Zhang, F. Brandao, and D. Suter, arXiv:1307.0257 (2013).
- [69] B. Smeltzer, L. Childress, and A. Gali, *New Journal of Physics* **13**, 025021 (2011).
- [70] C. S. Shin, M. C. Butler, H.-J. Wang, C. E. Avalos, S. J. Seltzer, R.-B. Liu, A. Pines, and V. S. Bajaj, *Physical Review B* **89**, 205202 (2014).
- [71] J. D. Wood, D. A. Broadway, L. T. Hall, A. Stacey, D. A. Simpson, J.-P. Tetienne, and L. C. Hollenberg, *Physical Review B* **94**, 155402 (2016).
- [72] C. P. Slichter, *Principles of magnetic resonance*, vol. 1 (Springer Science & Business Media, 2013).
- [73] E. van Oort, P. Stroomeer, and M. Glasbeek, *Physical Review B* **42**, 8605 (1990).
- [74] C. Cohen-Tannoudji, J. Dupont-Roc, and G. Grynberg, *Atom-Photon Interactions: Basic Processes and Applications*, by Claude Cohen-Tannoudji, Jacques Dupont-Roc, Gilbert Grynberg, pp. 678. ISBN 0-471-29336-9. Wiley-VCH, March 1998. p. 678 (1998).
- [75] R. Hanson, F. Mendoza, R. Epstein, and D. Awschalom, *Physical review letters* **97**, 087601 (2006).
- [76] A. Bermudez, F. Jelezko, M. Plenio, and A. Retzker, *Physical review letters* **107**, 150503 (2011).
- [77] M. Kohl, M. Odehnal, V. Petříček, R. Tichý, and S. Šafřata, *Journal of low temperature physics* **72**, 319 (1988).
- [78] H. Cheng, *Phys. Rev.* **124**, 1359 (1961), URL <https://link.aps.org/doi/10.1103/PhysRev.124.1359>.
- [79] J. Daycock and G. P. Jones, *Journal of Physics C: Solid State Physics* **2**, 998 (1969).

- [80] B. Alekseev, Radiophysics and Quantum Electronics **18**, 1272 (1975).
- [81] G. Varada and G. Agarwal, Physical Review A **45**, 6721 (1992).
- [82] J. R. Schrieffer and P. A. Wolff, Phys. Rev. **149**, 491 (1966).